Selective and Biocompatible Detection of Acetylcholine with a Fluorous Potentiometric Laser-Induced Graphene Sensor

Farbod Amirghasemi, Abdulrahman Al-Shami, Kara Ushijima, and Maral P. S. Mousavi*

Alfred E. Mann Department of Biomedical Engineering, Viterbi School of Engineering, University of Southern California, Los Angeles, CA, United States

E-mail: mousavi.maral@usc.edu

Phone: +123 (0)123 4445556. Fax: +123 (0)123 4445557

Abstract

Acetylcholine (ACh) appears in the brain and body of mammalians and functions both as a neuromuscular transmitter and neuromodulator. Tools with high spatial and temporal resolution to study ACh are in high demand due to the diverse function of ACh and its implications in neurodegenerative diseases. This work presents a highly promising sensor for a selective and biocompatible recording of ACh with a fluorous-phase potentiometric sensor. Fluorous compounds are nonpolar and not miscible with water and hydrocarbons, making them bio-orthogonal and biocompatible. This work presents the first proof-of-concept detection of ACh using a fluorous sensing phase. We show drastic improvement in selectivity for the fluorous-phase ion-exchanger electrode compared to a conventional ion-exchanger potentiometric sensor with a lipophilic sensing membrane. As a result, we observed more than an order of magnitude improvement in the limit of detection and two orders of magnitude increase in the electrode linear range during measurement of ACh in artificial cerebrospinal fluid. To enable the development of flexible and compact ACh sensing neural probes, this work combines the unique advantages of the fluorous-phase with a flexible laser-induced porous graphitic carbon (LIG) to create the first flexible solid-contact fluorous-phase potentiometric sensor. The fluorous-phase solid-contact LIG ion exchanger electrode showed a near Nernstian slope of 54.9 $\pm$ 0.8 and a 42 nM limit of detection.

Introduction

Acetylcholine (ACh) is an excitatory cholinergic neurotransmitter that acts primarily at neuromuscular junctions and motor ganglia synapses. In the central nervous system, ACh serves as a neuromodulator, impacting neuronal excitability and coordinating neuronal firing activity.[1] Abnormal ACh concentration in bodily fluids is associated with schizophrenia, Alzheimer's disease, and Parkinson's disease, among other illnesses.[2,3] Current sensing methods for ACh include mass spectroscopy, capillary electrophoresis, and liquid chromatography,[4–8] but these methods are highly expensive, slow, and lack relevance for real-time monitoring.[9] Other reported ACh detection methods utilized magnetic resonance imaging and fluorescence imaging using either ACh-quenching dyes or genetic probes based on activation of G protein-coupled receptors.[10–12] Limited optical access to deep brain structures and tissue damage due to bulky fiber optic systems remains a challenge for optical analysis of ACh.

Electrochemical sensing has been explored as an alternative detection method to access deep brain structures. Most electrochemical ACh sensors co-immobilized acetylcholinesterase and choline oxidase enzymes to convert ACh to hydrogen peroxide, followed by amperometric or voltammetric detection.[8,13–16] These electrodes have high selectivity but suffer from poor lifetime due to enzyme degradation. Recently, we and others have proposed the use of potentiometric sensing (relying on the permanent positive charge of ACh) to enable real-time ACh measurement without the need for an enzyme.[17–27] In this method, charge separation at the interface of the sensing membrane and sample generates an electrical potential that follows the Nernst equation. Selectivity is achieved via an organic receptor (ionophore) that is doped in the sensing membrane.[28] Most of the reported ionophores are highly stable and may result in ACh electrodes that can be used for long-term in-vivo recordings.[17–24,27,29] Potentiometric detection of ACh offers several advantages, such as a fast and non-destructive readout directly in the brain tissue or cerebrospinal fluid (CSF), enabling temporally resolved measurements in both chronic and acute settings.

ACh concentrations in brain tissue can range from 1 nM to 1 mM.[30] One of the major challenges that we have faced in potentiometric detection of ACh[17,29] has been poor limits of detection (21 μM[29]) in brain homogenate and CSF due to background signal from physiologically occurring ions. Development of new ionophores with higher selectivity for ACh over ions such as Na^+ that are present at high concentrations can improve the sensor LOD. A variety of ionophores were reported,[17–27] but they all incrementally differ in terms of selectivity. Successful nanomolar detection in CSF or brain tissue homogenate has not been achieved to date. The application of ACh potentiometric probes for in-vivo recordings has not been reported so far. An issue that we expect to observe during in-vivo chronic studies is biofouling of the electrodes, possibly due to electrode encapsulation by tissue, or ionophore and/or ionic site leaching (which may cause cytotoxicity), and extraction of lipophilic species into the sensing membrane.[31–35]

To resolve the aforementioned issues with electrode biofouling and sensor selectivity, this work presents the first proof-of-concept solid-contact ACh potentiometric sensor with a fluorous-phase ion-exchanger sensing membrane. Fluorous compounds (molecules with high content of fluorine atoms) are extremely non-polar and non-polarizable to the extent that they are not miscible with both aliphatic compounds such as hexanes, and with water and other hydrophilic compounds.[36] That is, fluorinated compounds are both hydrophobic and lipophobic. Living systems are made of water and lipophilic compounds, making fluorocarbons bio-orthogonal and nontoxic, meaning that they do not interfere with biology. Biocompatibility of fluorocarbons has resulted in many biomedical applications such as artificial blood, intraoperative tools for vitreoretinal surgery, bio-orthogonal imaging contrast agents, and delivery and imaging vehicles.[37–49] Fluorocarbons are used as coatings in biomedical devices to lower sensor biofouling and cell adhesion to the device.[50–56] This improvement on sensor biofouling is because the fluorous phase is significantly less polar than biological molecules such as lipids, making cell adhesion and biofilm formation difficult.

The application of fluorous materials for potentiometric sensing and development of fluo-

rophilic ionic sites and ionophores was invented by the Bühlmann research group.[57–66] To this end, they have developed fluorophilic ionophores for pH,[62,63] Ag^+,[64] and CO_3^{2-},[61] as well as fluorophilic cation[58] and anion exchangers.[65] It was demonstrated that a fluorous-phase ion exchanger electrode has a selectivity range that is seven orders of magnitude larger than the conventional potentiometric electrodes with a lipophilic sensing membrane.[65] Exceptional selectivities that far outperform a conventional lipophilic sensing membrane were also reported for ionophore-doped fluorous sensing membranes.[61–64] Such gain in selectivity is attributed to non-coordinating and poorly solvating properties of the fluorous phase.[61–65] In addition to the gain in selectivity, the authors pointed out another benefit of the fluorous-phase potentiometric sensors: increased resilience to biofouling compared to conventional sensors with a lipophilic membrane.[57–66] Preliminary studies on a fluorous-phase pH sensor[63] (exposed to diluted blood serum), and a rich literature on biocompatibility and biofouling resistance of fluorous compounds[37–49] supports this claim. Extensive studies should be performed to evaluate the biofouling resistance in both chronic and acute studies to better evaluate the feasibility of extended in-vivo studies with a fluorous-phase potentiometric sensor.

The high selectivity, biocompatibility, and potentially exceptional resilience to biofouling make fluorous-phase sensors ideal for neural applications. Neurotransmitters present in nanomolar concentrations are a complex matrix (requiring high selectivity). Moreover, studying the dynamics of change and the correlation of such changes to behavior and stimulation is desired (requiring long-term in-vivo studies through implantable sensors). Application of fluorous-phase potentiometric sensors was only explored for environmental monitoring of Ag^+ and perfluorinated surfactants.[67–70] This is likely due to the large sample (50-150 mL) volume required for measurements with fluorous-phase potentiometric sensors. Fluorous-phase sensors were fabricated using a custom-machined Kel-F electrode body that mechanically secures a porous Teflon disk (Fig. 1C).[63] This Teflon disk supports a liquid fluorous membrane containing the fluorophilic ion exchanger and ionic site. The electrode body also holds the inner-filling solution and the Ag-AgCl wire for signal transduction.[57–69]

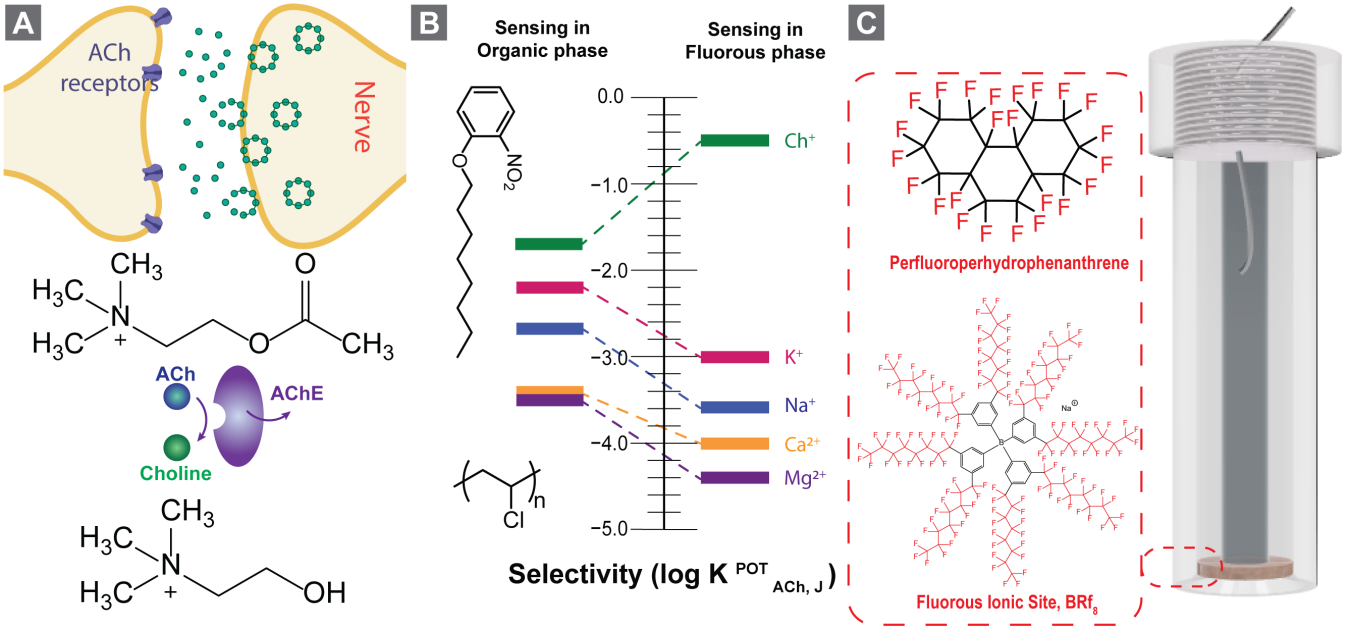

Figure 1: (A) Chemical strucutre of acetylcholine (ACh) and synaptic cleft of a neuromuscular junction. The enzyme acetylcholinesterase (AChE) converts the ACh to choline. (B) Comparison of selectivity for a fluorous-phase ion exchanger electrode and a conventional lipophilic potentiometric sensing membrane. (C) chemical structure of fluorous solvent and ionic site, and the KelF electrode body used for fabrication of fluorous-phase sensor.

In another example, the Kel-F electrode body supported a porous carbon monolith that is pressed against the Teflon disk to develop a solid-contact fluorous-phase potentiometric sensor for perfluorinated surfactants.[70]

In this work, we show the first use of a fluorous-phase potentiometric sensor for the measurement of ACh in CSF. The selectivity gain in the fluorous phase resulted in more than an order of magnitude improvement in the limit of detection (LOD). Moreover, to move towards in-vivo application of the fluorous-phase ACh sensor (where probe size and flexibility are critical), we have developed the first compact and flexible solid-contact fluorous-phase potentiometric sensor. We fabricated the electrodes using laser-induced carbonization of flexible polyimide films. Laser engraving is becoming a widely popular method for producing porous graphitic carbon structures, known as laser-induced graphene (LIG), for sensing applications.[71–73] LIGs are produced by ablating carbon-rich polymers (mostly polyimide) using a laser beam, which creates local photothermal reactions converting SP^3 carbon atom

hybridization into 3D porous graphitic structure.[74,75] This method is a maskless, scalable, reproducible, cost-effective, and fast approach to producing graphene layers with high electrical conductivity and electrocatalytic nature, which makes LIGs superior over graphene created using conventional methods such as chemical vapor deposition (CVD) and wet chemistry.[75–77] The combination of fluorous-phase potentiometric sensors with LIGs enables rapid and cost-effective prototyping of solid-contact sensors that are flexible and compact, opening up numerous opportunities for bio-analyses where sample volume is limited or a flexible form factor is needed. While there are numerous details to study and optimize related to fluorous-phase sensors and their utility for bio and neural applications, we wanted to share our current proof-of-concept results with the community and highlight the exciting opportunities in fluorous-phase sensing, specifically for ACh measurement.

Experimental Section

Materials

The fluorous ionic site (sodium tetrakis[3,5-bis(perfluoro-octyl)phenyl]borate, 3685.88 g/mol) was synthesized according to a previously published method.[59,63] Bis(trifluoromethyl)phenyl]borate (NaTFPB), 4-sulfocalix[4]arene (SCX4), 2-nitrophenyl octyl ether (o-NPOE), high-molecular-weight poly(vinyl chloride) (PVC), tetrahydrofuran (THF, inhibitor-free, HPLC Grade), perfluoroperhydrophenanthren, and choline chloride were purchased from Sigma Aldrich. EMD Millipore Fluoropore polytetrafluoroethylene (PTFE) membrane filters with pore size 0.45 μm, filter diameter 47 mm, thickness 50 μm, and 85% porosity were purchased from Fisher Scientific (Hanover Park, IL). All stock solutions with deionized water (resistivity of 18.2 MΩ·cm). Electrical grade polyimide films measuring 12 inches in width and 12 inches in length, with a thickness of 0.005 inches, were procured from McMaster-Carr, USA.

Electrochemical Measurements

All potentiometric measurements were conducted by utilizing a 16-channel potentiometer (Lawson Labs, Malvern, PA, USA) with 10.0 TΩ input impedance controlled with EMF Suite 1.03 software (Lawson Labs). All emf values were measured at room temperature (25±5 °C). We measured the emf values versus a commercial double junction free flow reference electrode (DX200, Mettler-Toledo) with 3.0 M KCl saturated with AgCl as the reference solution and 1.0 M lithium acetate as the bridge electrolyte. Calibration curves (Figs. 2, 3, and 6) were obtained by a series of half dilutions in either AChCl solution in deionized water or AChCl in a background of artificial CSF (a-CSF). The a-CSF solution based on previously published work comprising 145.0 mM NaCl, 2.7 mM KCl, 1.0 mM $MgSO_4$, 1.2 mM $CaCl_2$, 1.6 mM Na_2HPO_4, 0.5 mM NaH_2PO_4 and pH of 7.4 adjusted by HCl addition.[17] We determined the detection limit (LOD) by implementing the IUPAC recommendations (intersection between the Nernstian region and the plateaued section of the calibration curve).[78] The membrane resistivity (1.1 GΩ) was determined by the shunt method.[79] We monitored the emf change of the electrode before and after connecting a 1.0 GΩ resistor (SM104FE-1000M-ND, Ohmite, DigiKey, USA) in parallel to the working electrode and reference electrode (the electrodes were immersed in 10.0 mM AChCl solution during the measurement).

Selectivity coefficients were estimated by monitoring the emf of the fluorous-phase sensor in 100.0 μM AChCl for one minute, spiking the solution with 100 mM of the interfering ion, and re-recording the emf for one minute. The Nernst equation (1) was employed to calculate the selectivity coefficient. Electrochemical Impedance Spectroscopy (EIS) was conducted using CHI 760E potentiostat (CH Instruments, TX, USA). EIS was measured in a two-electrode setup 0.1 Hz to 100.0 kHz while applying an initial voltage of 100.0 mV with 0.5 V amplitude in a 10.0 mM AChCl solution against an Ag/AgCl reference electrode with porous Teflon frit (CHI 111, CH Instrument, Inc.). Cyclic voltammograms were measured from -0.2 to 0.6 V versus Ag/AgCl reference electrode (glass frit, 1 M KCl as reference solution) at scan rates of 20, 50, 80, and 100 mV/s in 2.0 mM $[Fe(CN)_6]^{3-/4-}$ and 100 mM KCl. A

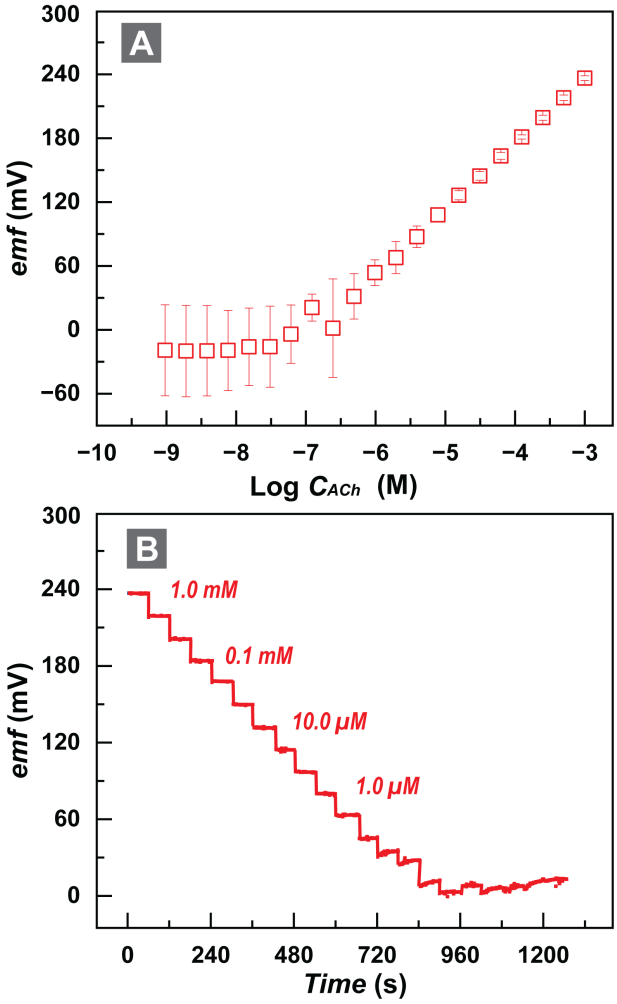

Figure 2: (A) Calibration curve of the fluorous-phase ACh sensor (0.1 mM AChCl and 0.1 mM KCl as inner-filling solution). Concentration of AChCl changed via successive dilutions from 1 mM to in 1.0 nM. (B) the corresponding emf trace over time for a representative electrode during calibration.

platinum wire was used as a counter electrode.

Fabrication of Graphitic Laser-Induced Carbon

We produced the laser-induced graphite electrodes (LIG) by ablating a polyimide film using a CO_2 laser cutter machine (EPILOG mini 24) with a 1060 nm laser wavelength in the presence of atmospheric air. The engraving was conducted with an auto-focused laser beam with power, engraving speed, and resolution of 3 W, 105 mm/s, and 1200 dots per inch

(DPI), respectively. Scanning electron microscopy (FEI NOVA nanoSEM 450) was utilized to investigate the topography of the LIG. Also, we employed the Raman spectroscopy technique using HORIBA XploRA microRaman Infrared Microscope to examine the carbon allotropes within the laser-irradiated region and assess the imperfections in the carbon lattice.

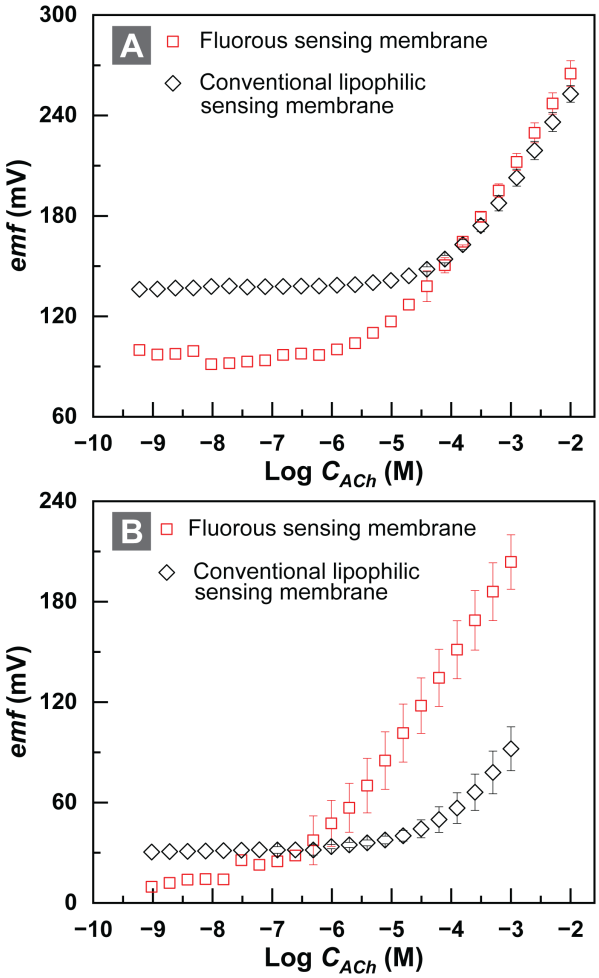

Figure 3: (A) Calibration curve of the fluorous-phase ACh sensor and conventional ion-exchanger electrode (both with 0.1 mM AChCl and 0.1 mM KCl as inner-filling solution) in aCSF. (B) Calibration curve of the fluorous-phase ACh sensor and conventional ion-exchanger electrode (both with a modified 1.0 mM ACh, 1.0 mM KCl, and 10.0 mM SCX4 inner-filling solution) in aCSF. Concentration of AChCl changed via successive dilutions from 1 mM to in 1.0 nM with aCSF. Black-lozenge shows the electrodes with a conventional lipophilic sensing membrane. Red-square shows the electrodes with a fluorous sensing membrane.

Electrode Fabrication

The liquid fluorous sensing phase was prepared by stirring 368.5 mg of fluorous ionic site (sodium tetra[perfluoro(octyl)butyl] bromide) in 0.5 mL of perfluoroperhy-drophenanthren (0.2 mM concentration) for 24 hours. A PCTFE-based electrode body (polychlorotrifluoroethylene, commonly known as Kel-F) was machined according to previously published design.[63] The machined electrode consists of three parts: screw cap, inner body, and sleeve (supporting information shows the pictures of the parts). We punched the PTFE membrane support to create 3/4" circular disks and sandwiched two layers of the PTFE membrane support between the inner electrode body and sleeve to secure the film. We added 10.0μL aliquots of the fluorous membrane on the PTFE membrane support to achieve a translucent color in the PTFE disk. We then filled the electrode body with an inner filling solution (IFS). The IFS contained 1.0 mM AChCl. The modified IFS contained 1.0 mM AChCl, 1.0 mM KCl, and 10.0 mM SCX4. We later positioned an Ag-AgCl wire inside the IFS and sealed the electrode body with parafilm to minimize the evaporation of IFS. The LIG fluorous electrodes were prepared by adding a single layer of the PTFE membrane support to cover the circular region of the LIG. We used a Kapton tape (with a punched hole in the middle) to seal the exposed LIG leads and secure the PTFE membrane to the polyimide film (supporting information shows the steps). We then added 2.0 μL of the liquid fluorous sensing phase to the PTFE membrane to achieve a translucent color. Both the fluorous body and LIG-based electrodes were conditioned in 1.0 mM AChCl solution for 24 hours. The lipophilic sensing membrane was prepared by dissolving 15.0 mg of NaTFPB, 495.0 mg of PVC, and 990.0 mg of o-NPOE in 4.5 mL of THF. The conventional lipophilic electrodes were prepared according to a previously described method (supporting information details the process).[17]

Results and Discussion

While we are developing a fluorophilic ACh ionophore, we wanted to test the performance of a fluorous ion-exchanger electrode for ACh sensing. Given the inherent selectivity of liquid-membrane and polymeric membrane potentiometric sensors for hydrophobic molecules, we hypothesized that an ion-exchanger fluorous electrode should be able to selectively measure ACh without a fluorophilic ionophore. We developed a fluorous-phase ion exchanger electrode using the fluorous ionic site of sodium tetrakis[3,5-bis(perfluoro-octyl)phenyl]borate. We synthesized this compound according to a previously published method.[59,63] Fig. 1C shows the electrode body design. Using a 1.0 mM AChCl inner-filling solution (IFS), we achieved a 60.8±3.4 mV/decade Nernstian slope and a 0.6 μM LOD (Fig. 2). Calibrations were performed after 24 h of conditioning in 1.0 mM AChCl. Fig. 2B shows the real-time emf values of a representative electrode over time, demonstrating signal stability and rapid equilibrium of emf after each dilution. We measured the membrane resistance using the shunt method and electrochemical impedance spectroscopy (EIS), and achieved a value of 1.1 GΩ, which is similar to previously reported membrane resistances for the fluorous system.[57–66] Since the primary application of the fluorous-phase ACh sensor is the measurement in the brain tissue, we calibrated the fluorous-phase sensors in a background of aCSF through successive dilutions. CSF has a high concentration of Na^+ (140-150 mM).[80]The experiments were repeated with a conventional potentiometric sensor with a PVC/NPOE ion exchanger membrane as a control.

Fig. 3A compares the performance of a fluorous-phase and PVC/NPOE-based sensing membrane in the background of a-CSF. The fluorous-phase electrode showed a slope of 60.2 ± 1.8 mV/decade and an LOD of 5.1 μM. The conventional ion-exchanger electrode had a sensitivity of 54.4 ± 0.8 mV/decade with LOD of 72.2 μM. The fluorous-phase electrode had a lower LOD and a linear range, which was approximately two orders of magnitude wider than the conventional lipophilic membrane electrode (Fig. 3A). This improvement is due to the higher selectivity of the fluorous-phase electrode for ACh over naturally occurring cations

such as Na^+. To further enhance the LOD of the potentiometric ACh electrodes, we modified the IFS to lower transmembrane fluxes that occur due to the concentration gradient between the sample and IFS. Since the baseline ACh in CSF is around sub-micromolar concentrations, we buffered the ACh in IFS around the same concentration using an organic calixarene ACh-complexing agent based on our previous work.[17] We observed an enhanced LOD for both platforms, achieving 1.0 μM for the fluorous-phase electrode and 45.6 μM for the lipophilic membrane electrode (Fig. 3B).

To confirm that the improved performance of the fluorous electrode in a-CSF is due to higher selectivity, we quantified the selectivity of the fluorous-phase and conventional electrodes for ACh^+ against naturally occurring ions such as Na^+, K^+, Ca^{2+}, Mg^{2+}, and choline (Ch^+). We attempted to measure selectivity coefficients using the separate solution method,[81] but we could not achieve the Nernstian slope for inorganic ions. To demonstrate higher selectivity of the fluorous system, we recorded the emf of the ACh electrode in 100.0 μM AChCl and then spiked the chloride salt of the interfering cation to achieve a 100 mM concentration in solution, along with the existing 100.0 μM AChCl, and recorded the emf again. Fig. 4 shows the results of this experiment. We calculated the estimated selectivity coefficients ($K^{POT}_{ACh,j}$) using the Nernst equation (Eq.1). The values are listed in Table 1. With the exception of ChCl, the emf of the lipophilic membrane potentiometric sensor increased much higher than that of the fluorous sensor, showing a lower selectivity for ACh over the spiked cations. For instance, after spiking 100 mM NaCl into the 100.0 μM AChCl solution, the emf of the lipophilic ion exchanger electrode increased by 26.6 mV, while the emf of the fluorous ion exchanger sensor decreased by -1.6 mV. The near order of magnitude gain in $K^{POT}_{ACh,Na}$ is instrumental in achieving a low LOD in a sodium-rich CSF matrix.

$$emf = E^\circ + \frac{RT}{z_{ACh}F} ln(a_{ACh} + \sum K^{POT}_{ACh,j} a_j^{z_{ACh}/z_j}) \quad (1)$$

Interestingly and unexpectedly, the fluorous ion exchanger electrode had the worst selectivity for ACh^+ over Ch^+ ($K^{POT}_{ACh,Ch}$ of -0.6) compared to the lipophilic ion exchanger

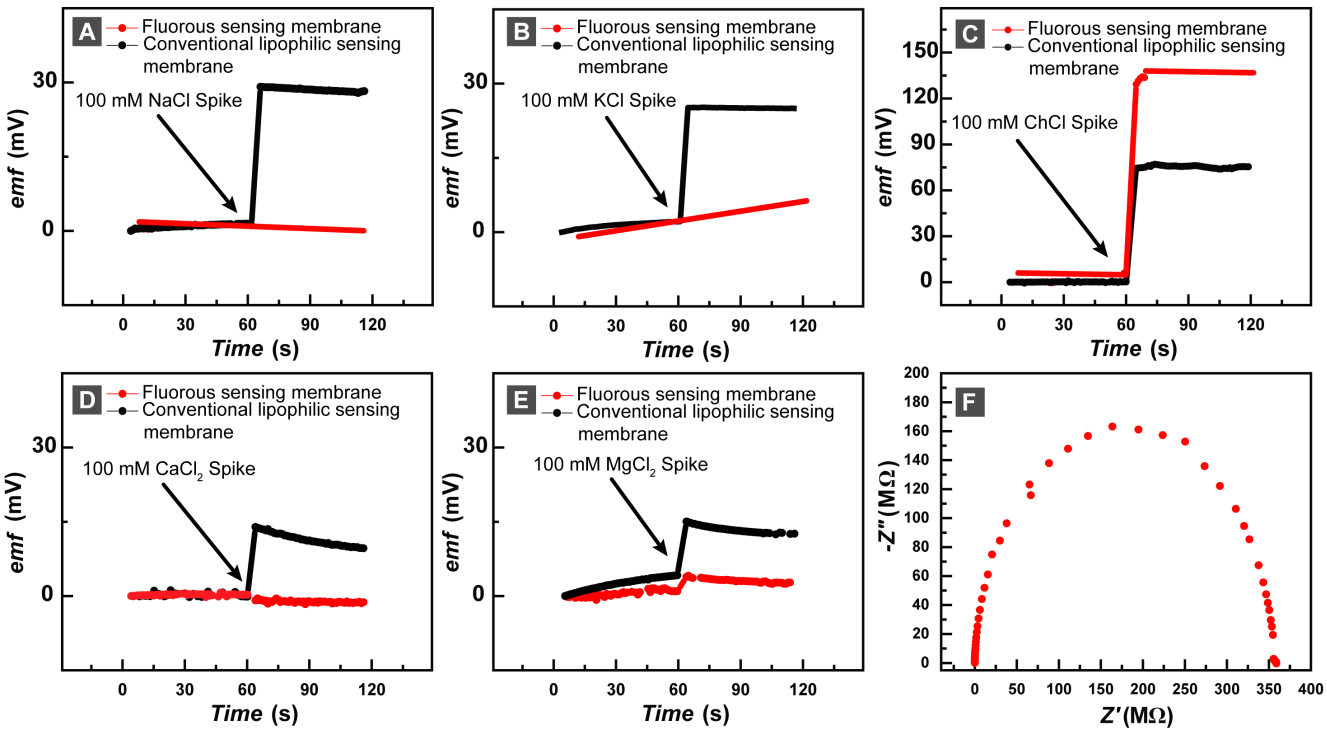

Figure 4: The emf of a representative fluorous-phase and conventional potentiometric sensor in 100.0 μM AChCl before and after spiking the solution with 100 mM of interfering cation of (A) sodium chloride, (B) potassium chloride, (C) choline chloride, (D) calcium chloride, and (E) magnesium chloride. The red trace shows the fluorous-phase electrode and the black trace shows the conventional lipophilic membrane electrode. (F) Impedance of the fluorous-phase electrode was ,measured in a 10 mM AChCl solution.

sensor ($K^{POT}_{ACh,Ch}$ of -1.7), as shown in Fig.4C. This may be due to the high hydrophobicity of the Ch^+ ion and different solvation properties compared to hydrophilic inorganic ions such as Na^+. We attempted to measure selectivity against a reference hydrophobic ion such as tetrabutylammonium (NBu_4^+), but even during the five-minute spiking experiment, the fluorous electrodes exhibited high drift (emf decreasing). We believe this drift was due to the exchange of ACh^+ in the fluorous membrane with NBu_4^+. Increasing the number of porous PTFE films to three in the electrode fabrication did not resolve this issue. Achieving high selectivity for ACh^+ over Ch^+ is critical for the ACh sensor because Ch^+ co-occurs with ACh^+ in the brain tissue and CSF. The poor selectivity of the fluorous electrode for ACh^+ over Ch^+ may be addressable by the development of fluorophilic ionophores. Future

Table 1: Selectivity Coefficient (K_{ij}^{POT}) for fluorous-phase and conventional sensing membrane. Measurements are for three replicates.

Interfering Ion	Fluorous Sensing Membrane	Lipophilic Sensing Membrane
Na^+	-3.6 ± 0.2	-2.7 ± 0.1
K^+	-3.1 ± 0.6	-2.2 ± 0.4
Ch^+	-0.6 ± 0.1	-1.7 ± 0.2
Ca^{2+}	-4.0 ± 0.2	-3.4 ± 0.2
Mg^{2+}	-4.4 ± 0.4	-3.4 ± 0.2

ionophore designs should specifically consider ionophore-ion interactions that differentiate between the hydroxyl and acetate end groups in Ch^+ and ACh^+.

The overall performance of the fluorous-phase ACh sensor shows great promise. One of the major issues for future application and extensive study of the system is the large and bulky electrode size and large sample volumes needed for each measurement. To address this issue, we developed a compact and flexible solid-contact fluorous ACh sensor using laser-induced graphitic carbon (LIG). These sensors are flexible, portable, and can be fabricated with the use of an inexpensive laser engraver. For future in-vivo applications, the electrode size and stiffness are important to minimize tissue damage during probe insertion and chronic readout.[82] LIG-based fluorous sensors can open up new avenues for both researching properties of fluorous-phase potentiometric electrodes and for exploring new applications for fluorous-phase potentiometry where sample volume is limited.

Fabrication and Characterization of Laser-induced Graphitic Carbon (LIG)

Engraving parameters including laser power, engraving speed, beam focusing, and resolution (dots per inch (DPI)), all impact the properties of laser-induced graphitic carbon (LIG). Higher laser power or a slower engraving process can improve graphene quality but risks overburning. Lower power, faster engraving, or smaller DPI value reduced the quality of produced graphite and, thereby, the electrochemical performance of the electrodes. Herein, we optimized the parameters and we found that a power of 3.0 W and speed of 105.0 mm/s

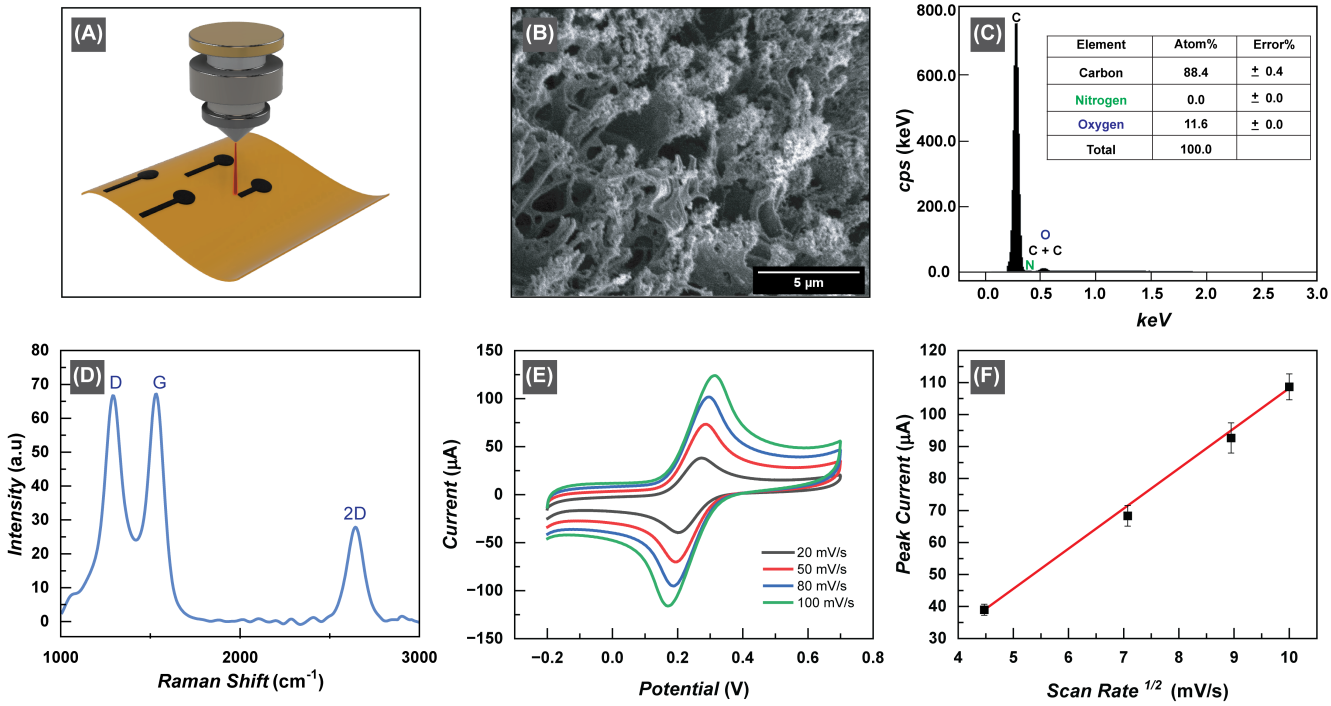

Figure 5: (A) Illustration of LIG fabrication using laser-induced carbonization. (B) SEM image of the LIG film (Scale: 5μm). (C) Energy Dispersive X-Ray (EDX) analy,sis of the LIG film. (D) Raman spectrum of the LIG film. (E) Cyclic voltammogram of 2.0 mM $[Fe(CN)_6]^{3-/4-}$ corresponding to different scan rates. (F) Linear relation of peak current with square root of scan rate, showing a diffusion controlled process.

at focus mode and with 1200 DPI are the optimal parameters to achieve high conductivity and device-to-device reproducibility and a stable carbon film (no mechanical delamination of the carbon from polyimide film). We used these parameters for the fabrication of the LIG-based electrodes in all the work.

We utilized scanning electron microscopy (SEM) to analyze the surface morphology of LIG. Fig. 5B illustrates the development of a highly porous and fibrous structure on the ablated region. This distinctive structure improves the adhesion between the electrode and the membrane as well as enhances the electrical capacitance at the electrode-membrane interface. We employed the energy-dispersive X-ray spectroscopy (EDX) technique to precisely quantify the elemental composition of the produced graphitic carbon material, as illustrated in Fig. 5C. The EDX analysis demonstrated that the surface of the LIG primarily comprises

of 88.4% carbon, with 11.6% oxygen, and no detectable nitrogen. This outcome confirms the effective conversion of the polyimide polymer into a graphitic form by laser inscribing. The oxygen content is ascribed to the engraving in an oxygen-rich environment and the high oxygen content of the polyimide film itself. Fig. 5D shows the Raman spectrum of the laser-engraved area. The 2D peak at $\approx$ 1638 cm^{-1} indicates graphene's presence; the G peak at $\approx$ 1534 cm^{-1} signifies vibrations in SP^2 carbon atoms, and the D peak at $\approx$ 1295 cm^{-1} suggests structural defects resulting from breaking within the graphene lattice.

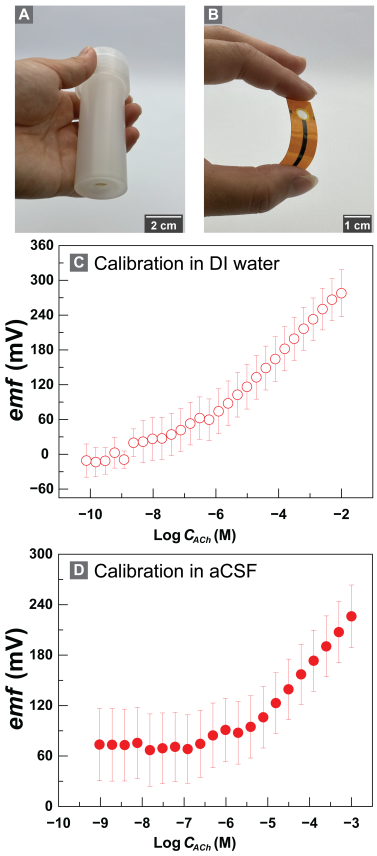

Figure 6: (A) Image of Kel-F electrode body used to fabricate fluorous-phase potentiometric electrodes. (B) Image of LIG solid-contact fluorous-phase potentiometric electrode (image taken before the fluorous phase is added to the Teflon film for better visibility). (C) Calibration curve of LIG solid-contact fluorous-phase potentiometric electrodes in AChCl solutions in deionized water. (D) Calibration curve of LIG solid-contact fluorous-phase potentiometric electrodes in AChCl solutions in a background of artificial cerebrospinal fluid (a-CSF).

In addition, we conducted cyclic voltammetry experiments to assess the electrochemical performance of the LIG-based electrodes. As depicted in Fig. 5E, voltammograms were

recorded at various scan rates, namely 20, 50, 80, and 100 mV/s. We observed an increase in both the oxidation current and reduction current, as well as an expanded peak separation with the scan rate increases. Furthermore, a linear correlation was established between the current peaks and the square root of the scan rate, implying a diffusion-controlled charge transfer process taking place on the electrode surface (Fig. 5F). This experiment was conducted on three different electrodes, and the recorded relative standard deviation (RSD) in peak current values was less than 4.5%, highlighting the high reproducibility of the fabrication process. To determine the active surface area of the electrodes, we employed the Randles–Sevcik equation.[83] The calculated active surface area of the LIG-based electrodes was approximately 2.3 ± 0.1 (n=3) times greater than the geometric area.

Fluorous-phase LIG Solid-contact Sensor

To fabricate the flexible solid-contact fluorous electrodes, we added a PTFE film support to the LIG, and secured it using Kapton tape (with a punched hole to expose the fluorous membrane to the sample). Fig. 6 shows the solid-contact fluorous-phase sensor (panel A) side by side the KelF body liquid-contact fluorous-phase sensor (panel B). Supporting information shows the photos of the sensor during each fabrication step. Fig. 6C demonstrates the calibration curve of the LIG fluorous ACh electrodes (n=3) in the range of 0.1 nM to 10.0 mM AChCl (concentration changed by serial dilutions). We achieved a sensitivity of 54.9±0.8 mV/decade and an LOD of 42 nM. Next, we assessed the performance of the LIG fluorous electrodes (n=3) in a-CSF, obtaining a LOD of 2.4 μM, and a slope of 59.4±2.2 mV/decade (Fig. 6D). As shown in Fig. 6C and D, there is a large sensor-to-sensor variability in the E^0 of the solid-contact LIG sensors. Supporting information shows the calibration curve of individual sensors, demonstrating that all the sensors are functional. We had fully characterized the LIG electrodes (prior to adding the membrane) and achieved high sensor-to-sensor reproducibility. Upon closer inspection, we noticed that during electrical connections (using a flat-head alligator clip), the carbon film was scratched on one of the electrodes, causing a

shift in response due to a change in the contact resistance. In future work, we will address the stability of electrical connections between the LIG film and the contact wire through the addition of other conductive inks that can mechanically strengthen the contact pad. The flexibility of the LIG electrodes has been confirmed in prior work for the development of wearable and electrochemical sensors.[76,84–86] We validated the flexibility of our bare LIG electrodes through measurement of electrode resistivity. After 0, 10, and 20 cycles of 180^0 bending of the electrodes, we obtained 201.2 ± 13.5 Ω/cm, 203.0 ± 7.0 Ω/cm, and 204.6 ± 10.0 Ω/cm, showing that electrode conductivity is retained. We repeated the bending experiment with the fluorous-phase LIG ACh sensors. We calibrated the LIG-based fluorous electrodes in aqueous ACh solutions with concentrations ranging from 0.625 mM − 10.0 mM. The sensitivity and E° values were 57.5 ± 2.2 mV/dec and 320.29 ± 17.2 mV before the bending test. After ten and twenty cycles of 180° bending, we measured a sensitivity of 62.3 ± 1.2 mV/decade and 62.6 ± 4.3 mV/decade, respectively. The E° values were 331.1 ± 19.1 mV and 343.6 ± 9.1 mV after ten and twenty bending cycles. These findings support that the resulting LIG fluorous ACh sensors are flexible. The E° changes could result from clipping and unclipping alligator clips from the electrodes during the calibration cycles.

The emf stability was measured in 1.0 mM AChCl for 12 h; the drift value was 10.3 μV/min. While we found this drift value acceptable for this proof-of-concept study, the stability should be improved in future work. We attempted to fabricate the fluorous LIGs without using the PTFE film, instead utilizing the porous structure of LIGs as a support for the liquid fluorous sensing cocktail. The electrodes exhibited large drifts and sub-Nernstian slopes. Direct use of LIG (without the PTFE support film) may be feasible in future work through further optimization to increase the LIG surface roughness and porosity.

Conclusions

Fluorous-phase sensors offer unprecedented selectivity and biocompatibility, but their application for bioanalyses has remained limited. This work demonstrated that an ionophore-free ion-exchanger fluorous-phase potentiometric sensor can be utilized for selective measurement of ACh in CSF. The selectivity arises from the inherent selectivity of membrane-based potentiometric sensors towards hydrophobic ions such as ACh. Because of the higher selectivity of the fluorous-phase sensors, the ion-exchanger fluorous ACh potentiometric sensor had a linear range (in a-CSF) that was two orders of magnitude higher than that of the conventional potentiometric electrode with a lipophilic PVC/NPOE membrane. An unexpected finding was that the fluorous-phase ACh ion exchanger had the worst selectivity for ACh^+ over Ch^+, suggesting that future efforts in ionophore design should focus on differentiating ionophore interactions with ACh^+ vs. Ch^+. This work also developed a proof-of-concept compact and flexible fluorous LIG potentiometric electrode. Independent of the target ion, this is the first report of a compact solid-contact fluorous potentiometric sensor. This platform enables a wide range of future studies on fluorous sensors as they can be measuredMembrane-to-LIG with a few microliters of sample volume.

While this study demonstrates the promise of a fluorous-phase potentiometric electrode for neural applications, there is still a long road ahead. Suitable fluorophilic ACh ionophores should be developed to enhance the selectivity and signal stability. Membrane-to-LIG adhesion should be improved to enhance the mechanical properties of the flexible probes. The LIG engraving parameters should be optimized for a fluorous-phase potentiometric application, as opposed to high conductivity and electron transfer kinetics (which have been the focus of most prior work on LIG electrochemical sensors). For instance, high surface roughness and hydrophobicity are desired in potentiometric measurements to minimize water-layer formation. The long-term stability of the fluorous LIG electrodes should be studied in CSF and tissue homogenate to determine the advantages over conventional lipophilic sensing membranes.

Acknowledgement

This work was funded by NIH Director's New Innovator Award (DP2GM150018), and Center for Autonomic Nerve Recording and Stimulation Systems (CARSS, 1U41NS129514-01). All authors thank the Core Center of Excellence in Nano Imaging at the University of Southern California. A. Al-Shami was funded by the Viterbi Graduate Fellowship from the University of Southern California. We thank Prof. Philippe Bühlmann and Xin Chen from the University of Minnesota for sharing the design files for the Kel-F electrode body and for insightful conversations on electrode machining.

References

(1) Picciotto, M. R.; Higley, M. J.; Mineur, Y. S. Acetylcholine as a neuromodulator: cholinergic signaling shapes nervous system function and behavior. *Neuron* **2012**, *76*, 116–129.

(2) White, K. E.; Cummings, J. L. Schizophrenia and Alzheimer's disease: clinical and pathophysiologic analogies. *Comprehensive psychiatry* **1996**, *37*, 188–195.

(3) Bohnen, N. I.; Yarnall, A. J.; Weil, R. S.; Moro, E.; Moehle, M. S.; Borghammer, P.; Bedard, M.-A.; Albin, R. L. Cholinergic system changes in Parkinson's disease: emerging therapeutic approaches. *The Lancet Neurology* **2022**,

(4) Singh, A. K.; Drewes, L. R. Improved analysis of acetylcholine and choline in canine brain and blood samples by capillary gas chromatography—mass spectrometry. *Journal of Chromatography B: Biomedical Sciences and Applications* **1985**, *339*, 170–174.

(5) Persike, M.; Zimmermann, M.; Klein, J.; Karas, M. Quantitative determination of acetylcholine and choline in microdialysis samples by MALDI-TOF MS. *Analytical chemistry* **2010**, *82*, 922–929.

(6) Song, P.; Hershey, N. D.; Mabrouk, O. S.; Slaney, T. R.; Kennedy, R. T. Mass spectrometry "sensor" for in vivo acetylcholine monitoring. *Analytical chemistry* **2012**, *84*, 4659–4664.

(7) Lamy, E.; Pilyser, L.; Paquet, C.; Bouaziz-Amar, E.; Grassin-Delyle, S. High-sensitivity quantification of acetylcholine and choline in human cerebrospinal fluid with a validated LC-MS/MS method. *Talanta* **2021**, *224*, 121881.

(8) Perry, M.; Li, Q.; Kennedy, R. T. Review of recent advances in analytical techniques for the determination of neurotransmitters. *Analytica chimica acta* **2009**, *653*, 1–22.

(9) Fenoy, G. E.; Marmisollé, W. A.; Azzaroni, O.; Knoll, W. Acetylcholine biosensor based on the electrochemical functionalization of graphene field-effect transistors. *Biosensors and Bioelectronics* **2020**, *148*, 111796.

(10) Luo, Y.; Kim, E. H.; Flask, C. A.; Clark, H. A. Nanosensors for the chemical imaging of acetylcholine using magnetic resonance imaging. *ACS nano* **2018**, *12*, 5761–5773.

(11) Jing, M.; Li, Y.; Zeng, J.; Huang, P.; Skirzewski, M.; Kljakic, O.; Peng, W.; Qian, T.; Tan, K.; Zou, J., et al. An optimized acetylcholine sensor for monitoring in vivo cholinergic activity. *Nature methods* **2020**, *17*, 1139–1146.

(12) Gu, X.; Wang, X. An overview of recent analysis and detection of acetylcholine. *Analytical Biochemistry* **2021**, *632*, 114381.

(13) Hou, S.; Ou, Z.; Chen, Q.; Wu, B. Amperometric acetylcholine biosensor based on self-assembly of gold nanoparticles and acetylcholinesterase on the sol–gel/multi-walled carbon nanotubes/choline oxidase composite-modified platinum electrode. *Biosensors and Bioelectronics* **2012**, *33*, 44–49.

(14) Vanỳsek, P.; Behrendt, M. Investigation of acetylcholine, choline and acetyl-

cholinesterase at the interface of the two immiscible electrolyte solutions. *Journal of Electroanalytical Chemistry and Interfacial Electrochemistry* **1981**, *130*, 287–292.

(15) Colombo, M. L.; Sweedler, J. V.; Shen, M. Nanopipet-based liquid–liquid interface probes for the electrochemical detection of acetylcholine, tryptamine, and serotonin via ionic transfer. *Analytical chemistry* **2015**, *87*, 5095–5100.

(16) Gulaboski, R.; Pereira, C. M.; Cordeiro, M. N. D.; Bogeski, I.; Ferreira, E.; Ribeiro, D.; Chirea, M.; Silva, A. F. Electrochemical study of ion transfer of acetylcholine across the interface of water and a lipid-modified 1, 2-dichloroethane. *The Journal of Physical Chemistry B* **2005**, *109*, 12549–12559.

(17) Mousavi, M. P.; Abd El-Rahman, M. K.; Mahmoud, A. M.; Abdelsalam, R. M.; Buhlmann, P. In situ sensing of the neurotransmitter acetylcholine in a dynamic range of 1 nM to 1 mM. *ACS sensors* **2018**, *3*, 2581–2589.

(18) Jaramillo, A.; Lopez, S.; Justice Jr, J. B.; Salamone, J. D.; Neil, D. B. Acetycholine and choline ion-selective microelectrodes. *Analytica Chimica Acta* **1983**, *146*, 149–159.

(19) Kim, H.; Oh, J.; Jeon, W. S.; Selvapalam, N.; Hwang, I.; Ko, Y. H.; Kim, K. A new cucurbit [6] uril-based ion-selective electrode for acetylcholine with high selectivity over choline and related quaternary ammonium ions. *Supramolecular Chemistry* **2012**, *24*, 487–491.

(20) Li, L.; Zhang, Y.; Du, P.; Qian, Y.; Zhang, P.; Guo, Q. Polymeric membrane electrodes using calix [4] pyrrole bis/tetra-phosphonate cavitands as ionophores for potentiometric acetylcholine sensing with high selectivity. *Analytical Chemistry* **2020**, *92*, 14740–14746.

(21) Liu, B.; Yang, Y.-H.; Wu, Z.-Y.; Wang, H.; Shen, G.-L.; Yu, R.-Q. A potentiometric acetylcholinesterase biosensor based on plasma-polymerized film. *Sensors and Actuators B: Chemical* **2005**, *104*, 186–190.

(22) Ashmawy, N. H.; Almehizia, A. A.; Youssef, T. A.; Amr, A. E.-G. E.; Al-Omar, M. A.; Kamel, A. H. Novel Carbon/PEDOT/PSS-Based screen-printed biosensors for acetylcholine neurotransmitter and acetylcholinesterase detection in human serum. *Molecules* **2019**, *24*, 1539.

(23) Poels, I.; Nagels, L. Potentiometric detection of amines in ion chromatography using macrocycle-based liquid membrane electrodes. *Analytica chimica acta* **2001**, *440*, 89–98.

(24) Khaled, E.; Hassan, H.; Mohamed, G. G.; Ragab, F. A.; Seleim, A. E. A. β-Cyclodextrin-based potentiometric sensors for flow-injection determination of acetylcholines. *Int. J. Electrochem. Sci* **2010**, *5*, 448–458.

(25) Kamel, A. H.; Al Hamid, F. A.; Soror, T. Y.; Galal, H. R.; El Gendy, F. A. Solid Contact Biosensor Based On Man-Tailored Polymers For Acetylcholine Detection: Application To Acetylcholinesterase Assay. *Eur. Chem. Bull* **2015**, *5*, 266–273.

(26) Sacramento, A. S.; Moreira, F. T.; Guerreiro, J. L.; Tavares, A. P.; Sales, M. G. F. Novel biomimetic composite material for potentiometric screening of acetylcholine, a neurotransmitter in Alzheimer's disease. *Materials Science and Engineering: C* **2017**, *79*, 541–549.

(27) He, C.; Wang, Z.; Wang, Y.; Hu, R.; Li, G. Nonenzymatic all-solid-state coated wire electrode for acetylcholine determination in vitro. *Biosensors and Bioelectronics* **2016**, *85*, 679–683.

(28) Bühlmann, P.; Pretsch, E.; Bakker, E. Carrier-based ion-selective electrodes and bulk optodes. 2. Ionophores for potentiometric and optical sensors. *Chemical Reviews* **1998**, *98*, 1593–1688.

(29) Amirghasemi, F.; Soleimani, A.; Bawarith, S.; Tabassum, A.; Morrel, A.; Mousavi, M. P. FAST (Flexible Acetylcholine Sensing Thread): Real-Time Detection

of Acetylcholine with a Flexible Solid-Contact Potentiometric Sensor. *Bioengineering* **2023**, *10*, 655.

(30) Blokland, A. Acetylcholine: a neurotransmitter for learning and memory? *Brain Research Reviews* **1995**, *21*, 285–300.

(31) Dinten, O.; Spichiger, U. E.; Chaniotakis, N.; Gehrig, P.; Rusterholz, B.; Morf, W. E.; Simon, W. Lifetime of neutral-carrier-based liquid membranes in aqueous samples and blood and the lipophilicity of membrane components. *Analytical chemistry* **1991**, *63*, 596–603.

(32) Bakker, E.; Pretsch, E. Lipophilicity of tetraphenylborate derivatives as anionic sites in neutral carrier-based solvent polymeric membranes and lifetime of corresponding ion-selective electrochemical and optical sensors. *Analytica chimica acta* **1995**, *309*, 7–17.

(33) Canovas, R.; Padrell Sanchez, S.; Parrilla, M.; Cuartero, M.; Crespo, G. A. Cytotoxicity study of ionophore-based membranes: Toward on-body and in vivo ion sensing. *ACS sensors* **2019**, *4*, 2524–2535.

(34) Zdrachek, E.; Bakker, E. Potentiometric sensing. *Analytical chemistry* **2020**, *93*, 72–102.

(35) Radomska, A.; Singhal, S.; Ye, H.; Lim, M.; Mantalaris, A.; Yue, X.; Drakakis, E. M.; Toumazou, C.; Cass, A. E. Biocompatible ion selective electrode for monitoring metabolic activity during the growth and cultivation of human cells. *Biosensors and Bioelectronics* **2008**, *24*, 435–441.

(36) Gladysz, J. A.; Curran, D. P.; Horváth, I. T. *Handbook of fluorous chemistry*; John Wiley & Sons, 2006.

(37) Patrick, M. J.; Janjic, J. M.; Teng, H.; O'Hear, M. R.; Brown, C. W.; Stokum, J. A.; Schmidt, B. F.; Ahrens, E. T.; Waggoner, A. S. Intracellular pH measurements using perfluorocarbon nanoemulsions. *Journal of the American Chemical Society* **2013**, *135*, 18445–18457.

(38) Sletten, E. M.; Swager, T. M. Readily accessible multifunctional fluorous emulsions. *Chemical Science* **2016**, *7*, 5091–5097.

(39) Yokoyama, K. Effect of perfluorochemical (PFC) emulsion on acute carbon monoxide poisoning in rats. *The Japanese journal of surgery* **1978**, *8*, 342–352.

(40) Vorob'ev, S. First-and second-generation perfluorocarbon emulsions. *Pharmaceutical Chemistry Journal* **2009**, *43*, 209–218.

(41) Janjic, J. M.; Ahrens, E. T. Fluorine-containing nanoemulsions for MRI cell tracking. *Wiley Interdisciplinary Reviews: Nanomedicine and Nanobiotechnology* **2009**, *1*, 492–501.

(42) Ahrens, E. T.; Flores, R.; Xu, H.; Morel, P. A. In vivo imaging platform for tracking immunotherapeutic cells. *Nature biotechnology* **2005**, *23*, 983–987.

(43) O'Hanlon, C. E.; Amede, K. G.; Meredith, R.; Janjic, J. M. NIR-labeled perfluoropolyether nanoemulsions for drug delivery and imaging. *Journal of fluorine chemistry* **2012**, *137*, 27–33.

(44) Yu, Q.; Liu, K.; Su, L.; Xia, X.; Xu, X., et al. Perfluorocarbon liquid: its application in vitreoretinal surgery and related ocular inflammation. *BioMed Research International* **2014**, *2014*.

(45) Day, R. A.; Estabrook, D. A.; Logan, J. K.; Sletten, E. M. Fluorous photosensitizers enhance photodynamic therapy with perfluorocarbon nanoemulsions. *Chemical Communications* **2017**, *53*, 13043–13046.

(46) Lowe, K. C. Blood substitutes: from chemistry to clinic. *Journal of materials chemistry* **2006**, *16*, 4189–4196.

(47) Guinovart, T.; Hernández-Alonso, D.; Adriaenssens, L.; Blondeau, P.; Rius, F. X.; Ballester, P.; Andrade, F. J. Characterization of a new ionophore-based ion-selective electrode for the potentiometric determination of creatinine in urine. *Biosensors and bioelectronics* **2017**, *87*, 587–592.

(48) Riess, J. G.; Krafft, M. P. Advanced fluorocarbon-based systems for oxygen and drug delivery, and diagnosis. *Artificial Cells, Blood Substitutes, and Biotechnology* **1997**, *25*, 43–52.

(49) Ruiz-Cabello, J.; Walczak, P.; Kedziorek, D. A.; Chacko, V. P.; Schmieder, A. H.; Wickline, S. A.; Lanza, G. M.; Bulte, J. W. In vivo "hot spot" MR imaging of neural stem cells using fluorinated nanoparticles. *Magnetic Resonance in Medicine: An Official Journal of the International Society for Magnetic Resonance in Medicine* **2008**, *60*, 1506–1511.

(50) Falde, E. J.; Yohe, S. T.; Colson, Y. L.; Grinstaff, M. W. Superhydrophobic materials for biomedical applications. *Biomaterials* **2016**, *104*, 87–103.

(51) Ameduri, B. Fluoropolymers: the right material for the right applications. *Chemistry–A European Journal* **2018**, *24*, 18830–18841.

(52) Li, S.; Guo, Z.; Zhang, H.; Li, X.; Li, W.; Liu, P.; Ren, Y.; Li, X. Abc triblock copolymers antibacterial materials consisting of fluoropolymer and polyethylene glycol antifouling block and quaternary ammonium salt sterilization block. *ACS Applied Bio Materials* **2021**, *4*, 3166–3177.

(53) Hirao, A.; Sugiyama, K.; Yokoyama, H. Precise synthesis and surface structures of architectural per-and semifluorinated polymers with well-defined structures. *Progress in polymer science* **2007**, *32*, 1393–1438.

(54) Campoccia, D.; Montanaro, L.; Arciola, C. R. A review of the biomaterials technologies for infection-resistant surfaces. *Biomaterials* **2013**, *34*, 8533–8554.

(55) Wang, Z.; Zuilhof, H. Antifouling properties of fluoropolymer brushes toward organic polymers: the influence of composition, thickness, brush architecture, and annealing. *Langmuir* **2016**, *32*, 6571–6581.

(56) Movsesian, N.; Hirth, S.; Speros, J.; Gupta, M. Robust vapor-deposited antifouling fluoropolymer coatings for stainless steel polymerization reactor components. *Industrial & Engineering Chemistry Research* **2020**, *59*, 15264–15270.

(57) Boswell, P. G.; Szíjjártó, C.; Jurisch, M.; Gladysz, J. A.; Rábai, J.; Bühlmann, P. Fluorophilic Ionophores for Potentiometric pH Determinations with Fluorous Membranes of Exceptional Selectivity. *Analytical Chemistry* **2008**, *80*, 2084–2090, Publisher: American Chemical Society.

(58) Boswell, P. G.; Anfang, A. C.; Bühlmann, P. Preparation of a highly fluorophilic phosphonium salt and its use in a fluorous anion-exchanger membrane with high selectivity for perfluorinated acids. *Journal of fluorine chemistry* **2008**, *129*, 961–967.

(59) Boswell, P. G.; Lugert, E. C.; Rábai, J.; Amin, E. A.; Bühlmann, P. Coordinative properties of highly fluorinated solvents with amino and ether groups. *Journal of the American Chemical Society* **2005**, *127*, 16976–16984.

(60) Boswell, P. G.; Bühlmann, P. Fluorous Bulk Membranes for Potentiometric Sensors with Wide Selectivity Ranges: Observation of Exceptionally Strong Ion Pair Formation. *Journal of the American Chemical Society* **2005**, *127*, 8958–8959, Publisher: American Chemical Society.

(61) Chen, L. D.; Mandal, D.; Pozzi, G.; Gladysz, J. A.; Buhlmann, P. Potentiometric sensors based on fluorous membranes doped with highly selective ionophores for carbonate. *Journal of the American Chemical Society* **2011**, *133*, 20869–20877.

(62) Boswell, P. G.; Szíjjártó, C.; Jurisch, M.; Gladysz, J. A.; Rabai, J.; Bühlmann, P. Fluorophilic ionophores for potentiometric pH determinations with fluorous membranes of exceptional selectivity. *Analytical chemistry* **2008**, *80*, 2084–2090.

(63) Chen, X. V.; Mousavi, M. P.; Bühlmann, P. Fluorous-Phase Ion-Selective pH Electrodes: Electrode Body and Ionophore Optimization for Measurements in the Physiological pH Range. *ACS Omega* **2020**, *5*, 13621–13629, Publisher: American Chemical Society.

(64) Lai, C.-Z.; Fierke, M. A.; da Costa, R. C.; Gladysz, J. A.; Stein, A.; Buhlmann, P. Highly selective detection of silver in the low ppt range with ion-selective electrodes based on ionophore-doped fluorous membranes. *Analytical chemistry* **2010**, *82*, 7634–7640.

(65) Boswell, P. G.; Bühlmann, P. Fluorous bulk membranes for potentiometric sensors with wide selectivity ranges: Observation of exceptionally strong ion pair formation. *Journal of the American Chemical Society* **2005**, *127*, 8958–8959.

(66) Lai, C.-Z.; Reardon, M. E.; Boswell, P. G.; Bühlmann, P. Cation-coordinating properties of perfluoro-15-crown-5. *Journal of fluorine chemistry* **2010**, *131*, 42–46.

(67) Mousavi, M. P.; Gunsolus, I. L.; De Jesús, C. E. P.; Lancaster, M.; Hussein, K.; Haynes, C. L.; Bühlmann, P. Dynamic silver speciation as studied with fluorous-phase ion-selective electrodes: Effect of natural organic matter on the toxicity and speciation of silver. *Science of the Total Environment* **2015**, *537*, 453–461.

(68) Gunsolus, I. L.; Mousavi, M. P.; Hussein, K.; Buhlmann, P.; Haynes, C. L. Effects of humic and fulvic acids on silver nanoparticle stability, dissolution, and toxicity. *Environmental science & technology* **2015**, *49*, 8078–8086.

(69) Maurer-Jones, M. A.; Mousavi, M. P.; Chen, L. D.; Bühlmann, P.; Haynes, C. L. Characterization of silver ion dissolution from silver nanoparticles using fluorous-phase

ion-selective electrodes and assessment of resultant toxicity to Shewanella oneidensis. *Chemical Science* **2013**, *4*, 2564–2572.

(70) Chen, L. D.; Lai, C.-Z.; Granda, L. P.; Fierke, M. A.; Mandal, D.; Stein, A.; Gladysz, J. A.; Buhlmann, P. Fluorous membrane ion-selective electrodes for perfluorinated surfactants: Trace-level detection and in situ monitoring of adsorption. *Analytical chemistry* **2013**, *85*, 7471–7477.

(71) Johnson, Z. T.; Williams, K.; Chen, B.; Sheets, R.; Jared, N.; Li, J.; Smith, E. A.; Claussen, J. C. Electrochemical sensing of neonicotinoids using laser-induced graphene. *ACS sensors* **2021**, *6*, 3063–3071.

(72) Chen, B.; Johnson, Z. T.; Sanborn, D.; Hjort, R. G.; Garland, N. T.; Soares, R. R.; Van Belle, B.; Jared, N.; Li, J.; Jing, D., et al. Tuning the structure, conductivity, and wettability of laser-induced graphene for multiplexed open microfluidic environmental biosensing and energy storage devices. *ACS nano* **2021**, *16*, 15–28.

(73) Hjort, R. G.; Soares, R. R.; Li, J.; Jing, D.; Hartfiel, L.; Chen, B.; Van Belle, B.; Soupir, M.; Smith, E.; McLamore, E., et al. Hydrophobic laser-induced graphene potentiometric ion-selective electrodes for nitrate sensing. *Microchimica Acta* **2022**, *189*, 122.

(74) Lin, J.; Peng, Z.; Liu, Y.; Ruiz-Zepeda, F.; Ye, R.; Samuel, E. L.; Yacaman, M. J.; Yakobson, B. I.; Tour, J. M. Laser-induced porous graphene films from commercial polymers. *Nature communications* **2014**, *5*, 5714.

(75) Dixit, N.; Singh, S. P. Laser-induced graphene (LIG) as a smart and sustainable material to restrain pandemics and endemics: A perspective. *ACS omega* **2022**, *7*, 5112–5130.

(76) Wang, M.; Yang, Y.; Gao, W. Laser-engraved graphene for flexible and wearable electronics. *Trends in Chemistry* **2021**, *3*, 969–981.

(77) Lahcen, A. A.; Rauf, S.; Beduk, T.; Durmus, C.; Aljedaibi, A.; Timur, S.; Alshareef, H. N.; Amine, A.; Wolfbeis, O. S.; Salama, K. N. Electrochemical sensors and biosensors using laser-derived graphene: A comprehensive review. *Biosensors and Bioelectronics* **2020**, *168*, 112565.

(78) Lindner, E.; Umezawa, Y. Performance evaluation criteria for preparation and measurement of macro-and microfabricated ion-selective electrodes (IUPAC Technical Report). *Pure and Applied Chemistry* **2008**, *80*, 85–104.

(79) Oesch, U.; Simon, W. Lifetime of neutral carrier based ion-selective liquid-membrane electrodes. *Analytical Chemistry* **1980**, *52*, 692–700.

(80) Shiobara, R.; Ohira, T.; Doi, K.; Nishimura, M.; Kawase, T. Development of artificial cerebrospinal fluid: basic experiments, and phase II and III clinical trials. *J Neurol Neurophysiol* **2013**, *4*, 173.

(81) Bakker, E.; Pretsch, E.; Bühlmann, P. Selectivity of potentiometric ion sensors. *Analytical chemistry* **2000**, *72*, 1127–1133.

(82) Otte, E.; Vlachos, A.; Asplund, M. Engineering strategies towards overcoming bleeding and glial scar formation around neural probes. *Cell and Tissue Research* **2022**, *387*, 461–477.

(83) Griesche, C.; Hoecherl, K.; Baeumner, A. J. Substrate-independent laser-induced graphene electrodes for microfluidic electroanalytical systems. *ACS Applied Nano Materials* **2021**, *4*, 3114–3121.

(84) Yang, Y.; Song, Y.; Bo, X.; Min, J.; Pak, O. S.; Zhu, L.; Wang, M.; Tu, J.; Kogan, A.; Zhang, H., et al. A laser-engraved wearable sensor for sensitive detection of uric acid and tyrosine in sweat. *Nature biotechnology* **2020**, *38*, 217–224.

(85) Pinheiro, T.; Correia, R.; Morais, M.; Coelho, J.; Fortunato, E.; Sales, M. G. F.; Marques, A. C.; Martins, R. Water peel-off transfer of electronically enhanced, paper-based laser-induced graphene for wearable electronics. *ACS nano* **2022**, *16*, 20633–20646.

(86) Sain, S.; Roy, S.; Mathur, A.; Rajesh, V.; Banerjee, D.; Sarkar, B.; Roy, S. S. Electrochemical Sensors Based on Flexible Laser-Induced Graphene for the Detection of Paraquat in Water. *ACS Applied Nano Materials* **2022**, *5*, 17516–17525.

TOC Graphic